Optically Transparent Honeycomb Mesh Antenna Integrated into OLED Light Source

Mustapha El Halaoui, Pascal Dupuis, Olivier Pigaglio, Adel Asselman, Georges Zissis, Laurent Canale

Optically Transparent Honeycomb Mesh Antenna Integrated into OLEDs Light Source

Mustapha El Halaoui [1, 2], Pascal Dupuis [2], Olivier Pigaglio [2], Adel Asselman [1], Georges Zissis [2] and Laurent Canale [2,*]

[1] Optics, Material and Systems Team, Faculty of Sciences, Abdelmalek Essaadi University, P.O. Box: 2121, Tetouan, Morocco.
[2] Université Toulouse III – Paul Sabatier, LAPLACE, UMR 5213, (CNRS, INPT, UPS), 118 rte de Narbonne, 31062 Toulouse, France.
* Correspondence: canale@laplace.univ-tlse.fr

Abstract: The co-integration of antennas with lighting sources appears as an effective way to distribute broadband networks closest to users, lowering interference and transmitted power, as well as to reduce energy consumption in future lighting systems. We present here an original contribution to the implementation of transparent and invisible antennas on OLED light sources. To validate the proposed approach, the honeycomb mesh technique is used and optical transparency of 75.4 % is reached. The transparent mesh antenna is compared with the non-transparent full metal antenna in terms of radio-electrical parameters. Our prototype is designed by using copper films deposited on a glass substrate. Simulation results of the S-parameters and the radiation patterns are validated against measurements performed in an anechoic chamber. The directivity and the gain obtained are 6.67 dBi and 4.86 dBi at 5.16 GHz, respectively. To study the effect of the antenna integration on OLED, optical and photometric characterizations with and without antenna were measured and the colorimetric parameters were treated afterwards using the IES TM-30-18 standard.

Keywords: Antenna design; optically transparent antenna; mesh antenna; Organic Light Emitting Diodes (OLEDs); WLAN

1. Introduction

Due to its excellent integration qualities, high energy efficiency, low luminance without glare and potentially low manufacturing costs, OLEDs (Organic Light Emitting Diodes) could integrate easily into urban space for pedestrian lighting. Despite its maturity, manufacturers are still reluctant to invest massively in this technology as long as the LED market is booming. Nevertheless, in the last few years, OLEDs have rapidly progressed and commercially available models are already used in lighting and displays [1]. These developments are of great interest to manufacturers because it is obvious that this technology will be at the heart of the next generation of general lighting sources in smart cities [2]. Intelligence requires indeed new wireless network infrastructures to support the increase in the volume of communication linked to the new services. Furthermore, the installation of connected network between the smart city services needs a larger communication area. Therefore, it is necessary to install more antennas in the interface of all connected objects and to multiply the base stations in the city to achieve reliable communication [3]. Due to the miniaturization of these objects and the visual pollution caused by the installation of more base stations in cities, this requirement becomes difficult to fulfill [4]. For this reason, optically transparent antennas can be quite promising solution to replace non-transparent antennas. Because of their optical transparency, these antennas can be integrated into screens, glazing, bus stops, and OLED lamps, etc. More antennas means an improvement of network coverage without increasing the visual or spatial impacts linked to their presence [5,6].

With the expansion of the transparent device market, optically transparent antennas would have a great potential for newer wireless communication systems. The manufacturing process is based on the deposition of electrically conductive and transparent material on transparent substrates [7,8]. According to the literature, the transparent materials used in the manufacture of these antennas are: Indium Tin Oxide (ITO) [9–12], Fluorine doped Tin Oxide (FTO) [13], aluminum doped zinc oxide (AZO) [14], AgHT-4 [15,16], AgHT-8[17–20]), ultra-thin metal film [21], and mesh structures [22–28].

The development of mobile devices benefits from the integration of the antenna with the transparent and flexible screen display. The antenna-on-display (AoD) solution is already implemented in the literature on OLED and LCD (Liquid Crystal Displays) displays. The original concept of optically and invisible AoD has been studied and tested in high-resolution OLED touch displays for Wi-Fi and Bluetooth applications in smartwatch [29,30]. Furthermore, in [31] the authors presented a detailed study of an optically invisible antenna integrated into OLEDs and LCDs displays for smartphone. This antenna operates in the millimeter-wave (mm-Wave) band for 5G cellular applications. The diamond mesh and identical dummy-grids techniques are used to achieve the optical invisibility and transparency. Therefore, the dummy grids structures are diamond shaped encompassed the designed antenna region, to eliminate any difference in optical transmittance. Similarly, [32] also presents an AoD that can eventually be integrated into display panel for the sub-6 GHz band. In addition, a simulation study of optically transparent antennas that can be integrated into light source OLEDs is presented in [4,33,34]. All these studies were carried out to understand the operation of the antenna integrated into OLEDs without taking into consideration the effect of this integration on the displays color appearance.

This paper presents the design and realization of a transparent and invisible antenna, designed of a honeycomb mesh for the 5 GHz WLAN band. This study focuses on two main challenges in order to examine the antennas integration effects on OLEDs light source. The first is the transparent antenna design using the mesh technique. This analysis is based on a comparison between two antennas; a full metal antenna and a honeycomb meshed one. Honeycomb mesh technique is used to design the invisible and transparent antenna with high transparency and acceptable sheet resistance value. The second one is the antenna integration and its effects on the OLED panels visual characteristics. For this purpose, this paper aims to study the colorimetric parameters of warm white OLED after the integration of the transparent mesh antenna. It contains a physical realization of concepts analyzed in [34], which presented a comparative study of simulation results of the transparent circular patch antennas integrated into OLEDs. It is important to note that; the meshing technique to achieve optical transparency has been widely discussed in the literature [4,22–34]. However, this paper presents for the first time a complete study which contains the antenna electrical parameters and the colorimetric parameters of the screen before and after the antenna integration.

The remaining of this article is organized as follows: section 2 describes the material characteristics used in the design. To justify the choice of the transparent antenna, section 3 describes a comparison between this antenna and another non-transparent one. The experimental results are discussed and compared with simulation in section 4. The method of the antenna integration into an OLED light source and the effect of this integration on the radio-electrical parameters of the antenna and on the OLED colorimetric parameters are studied in section 5. Conclusions and perspectives are presented in section 6.

2. Material characteristic

This article proposes a study of a transparent antenna integrated into the OLED light source by providing connectivity for wireless communications. The proposed antenna is designed by transparent materials deposited in a glass substrate. In first step, the characteristics of the materials used in this design were studied. These parameters are: optical and dielectric parameters for the glass substrate, and the sheet resistance and the transparency for conductive materials.

2.1. Substrate characteristics

The main characteristics of interest are the optical transparency (Tsub), the dielectric permittivity (ϵ_r) and the tangent of the loss angle ($tan(\delta)$). The dielectric parameters were measured using Vector Network Analyzer associated to 85070B dielectric probe kit with a tolerance of $\pm 5\,\%$ and $\pm 0.05\,\%$ on dielectric permittivity and dielectric losses, respectively. The measurement results of ϵ_r and $tan(\delta)$ are shown in Fig. 1. According to this figure, the measured values at a frequency of 5.16 GHz are $\epsilon_r = 6.2$ and $tan(\delta) = 0.05$.

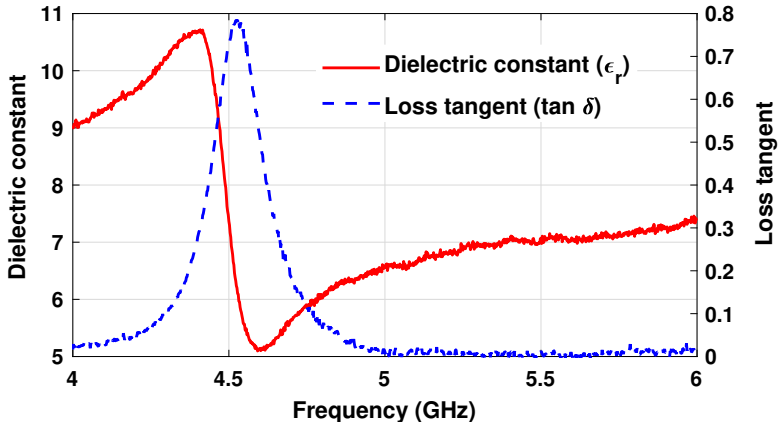

Figure 1. Dielectric permittivity and tangent of the loss angle.

The other studied parameter is the optical transparency in the visible spectrum. This parameter was measured using an optical bench at room temperature using a MINOLTA-CS-1000 spectroradiometer. In a first step, the OLED luminance was evaluated. In a second step, the glass substrate was inserted through a lentil holder in front of the objective, in order to intercept the whole luminous path. The transparency is the ratio of the latter luminance to the former at corresponding wavelength. Fig. 2 illustrates this optical transparency; the median value is approximatively 82.5 %. The noise below 480 nm results from the low emission in this band, leading to an increased noise level.

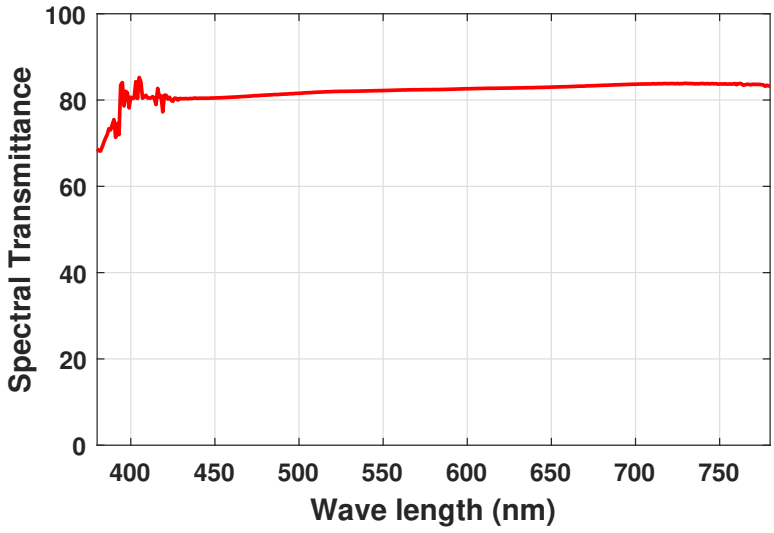

Figure 2. Optical transparency for glass substrate in the visible spectrum.

2.2. Sheet resistance

The two popular types of transparent antennas are meshed and TCOs-based antennas. In this work, ITO film and mesh structure are studied and compared. The sheet resistance $R_s(\Omega/sq)$ and transparency T (%) are compared to identify the most desirable material in this design.

2.2.1. ITO film

One of the widely used TCOs in the transparent antennas design is the ITO films. the ITO has considerable importance in the OLEDs manufacture because it is commonly used as electrode in OLEDs. Several researchers are using this material in optically transparent antenna fabrication [9,11,12]. It is a good choice due to its high optical transparency, but their high sheet resistance remains a challenge for researchers.

The resistance of a sheet is the electrical resistance of a square surface of a material of thickness t [6]. The sheet resistance of ITO film is given by this relation:

$$R_s = \frac{1}{\sigma \cdot t} \tag{1}$$

Where σ is the conductivity and t is the thickness of the ITO film.

2.2.2. Mesh structure

The metal mesh structure is a realization of the conductive films for optically transparent antennas. The principle of the mesh technique is to create holes in an opaque structure to allow light to pass. The transparency and the sheet resistance change with the surface variation of these holes. Fig. 3 represents the honeycomb-shaped structure chosen in this work. In general, the sheet resistance of the mesh structure is calculated by the equation [26]:

$$R_{s(mesh)} = \frac{q}{e} \times R_s \tag{2}$$

Where $R_s = 0.047\Omega/sq$ is the sheet resistance of the copper film (calculated by equation 1 with $\sigma = 5.8 \times 10^7 S/m$ and $t = 370\,\text{nm}$), q is the pitch value and e is the metal strip. Since the honeycomb structure is used, then the sheet resistance has been calculated in both axes OX and OY, in relation to the direction of current propagation in the mesh antenna. The resistances along each axis are given by the following relations:

$$R_{s(mesh)} = \frac{q_x}{e} \times R_s \; and \; R_{s(mesh)} = \frac{q_y}{e} \times R_s \tag{3}$$

The values of the chosen parameters are: $q_x = 0.32\,\text{mm}$, $q_y = 0.5\,\text{mm}$, $e = 0.05\,\text{mm}$ and $R_s = 0.047\Omega/sq$ (equation 1). Therefore, a value of approximately $R_s = 0.2\Omega/sq$ was obtained for the mesh. Note that this value is greater than the resistance of the copper film, but the use of these techniques increases the material transparency [22,26].

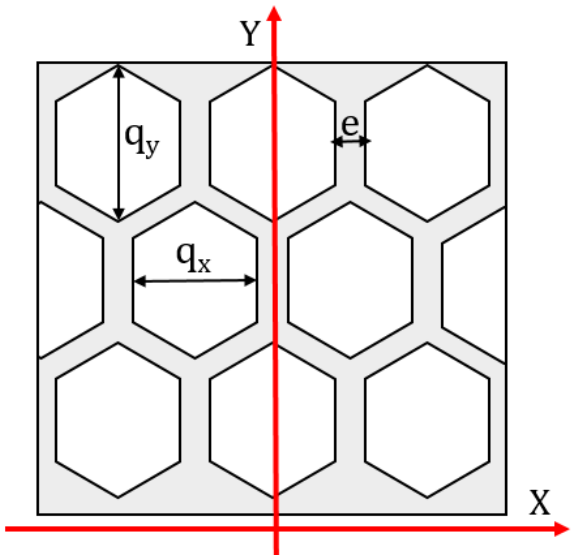

Figure 3. The geometry of the honeycomb mesh.

2.3. Optical transparency

The optical transparency is another parameter was studied. Fig. 4 illustrates a comparison between the optical transparency of the ITO film and the honeycomb mesh structure from 380 to 780 nm. Although large dimensions of the mesh are required to achieve high optical transparency, but this also increases the sheet resistance. From this figure, the mesh structure exhibits excellent transparency compared to ITO in the whole visible spectrum. The measured transparencies remain constant. The transparency median value of the mesh structure is approximately 75.4 %, while of the ITO film is 65.1 %. Note that, the measured transparencies are the transparency of two layers of the ITO and mesh structure deposited on the glass substrate.

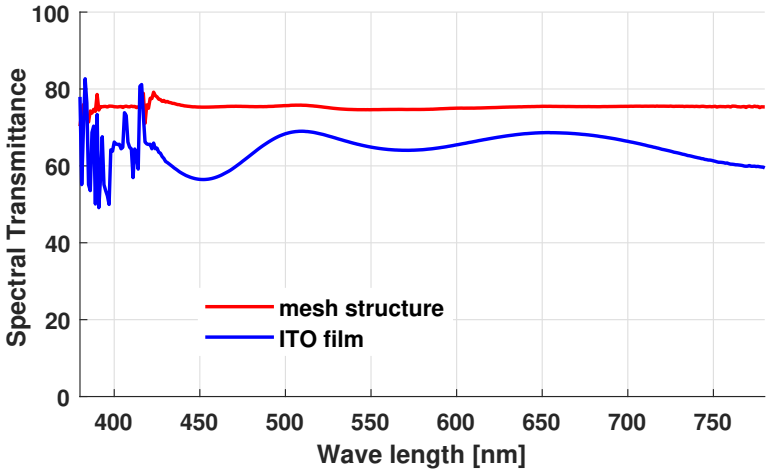

Figure 4. Comparison between the optical transparency for the ITO film and mesh structure in the visible spectrum.

The overall transparency results from the cascading of three layers: two meshed grids and the substrate. Assuming that the contributions of the grids are identical, we may determine the mesh contribution as:

$$T_{tot} = T_{mesh} \cdot T_{substr} \cdot T_{mesh} \tag{4}$$

$$T_{mesh} = \sqrt{\frac{T_{tot}}{T_{substr}}} \tag{5}$$

Inserting the previously measured transparency values in Eq 5, the transparency of the mesh can be evaluated to 95.5 %. That suggests that if the OLED glass substrate and its anode can be used as support and ground plane respectively, the impact of a single mesh layer would be quite small. This argument goes in favor of co-design and co-integration of the display and radiation functions.

2.4. Comparison between ITO and mesh technique

The transparency and sheet resistance comparison of ITO film and mesh structure are given in Table 1. From this table, the transparency of mesh structure is 13.67 % higher than that of ITO film, while its sheet resistance is 95.5 % lower than that of ITO. Therefore, the mesh structure is achieved the better performances in comparison with that of ITO film. In this article, the mesh structure was chosen to design the transparent antenna integrated into OLED light source.

Table 1. Comparison between ITO film and mesh structure.

	ITO film	Copper film	Mesh structure
Transparency (%)	65.1	opaque	75.4
Sheet resistance (Ω/sq)	4.51	0.047	0.2
Thickness (nm)	370	370	370

2.5. Invisibility to the bare eye

In order to integrate the mesh antenna into the OLED, the parameters of the honeycomb structure are optimized so that the human eye cannot distinguish the structure. The performances of the bare eye are considered in this optimization. Therefore, the eye angular discrimination is $\theta_{min} = 4.9 \times 10^{-4}$ rad [35]. The distance between two distinct points can be expressed as:

$$p_{min} = d \cdot \tan\theta_{min} \approx d \cdot \theta_{min} \quad (6)$$

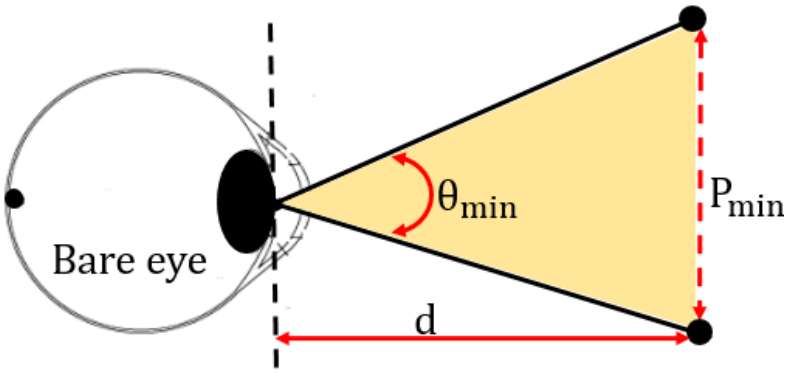

Figure 5. Diagram of the discrimination of two points observed with the bare eye [35].

The distance d between the eye and the object depends on the intended application in which the mesh will be used (Fig. 5). This distance is equal to the minimum punctum proximum value. Thus, a distance of 1 m was considered, which is quite sufficient for the antenna to be invisible in OLED light sources.

The calculated distance using equation 6 is approximately $p_{min} = 490\,\mu$m. We can conclude that the mesh antenna using these parameters will be invisible to the bare eye at a minimum distance of 1 m.

3. Antenna configurations

Two complementary case studies were implemented to investigate an antenna integrated into the OLED. The non-transparent antenna is designed with the full copper film. The optically transparent and invisible antenna make use of a honeycomb shaped mesh structure. The full-metal version serves as a reference standard for RF properties characterisation.

3.1. Non-transparent antennas

A reference non-transparent patch antenna is designed by full copper film in a first step. The geometry of the non-transparent antenna are depicted in Fig. 6. This antenna consists of a radiating element on one side of the glass substrate (with thickness $h_s = 1.1$ mm) and a ground plane on the other side.

The width ($W_f = 1.77$ mm) and the length ($L_f = 5.8$ mm) of the antennas feedline are calculated to match the characteristic impedance of $50\Omega/sq$. Both antennas occupy a volume of $25 \times 25 \times 1.1$ mm^3. Copper film (conductivity $\sigma = 5.8 \times 10^7 S/m$, thickness $t = 370$ nm and sheet resistance $R_s = 0.05\Omega/sq$) is used to design the two antennas. The

dimensions were calculated using the equations in [36], so that the antenna operate in the 5.15 GHz WLAN band.

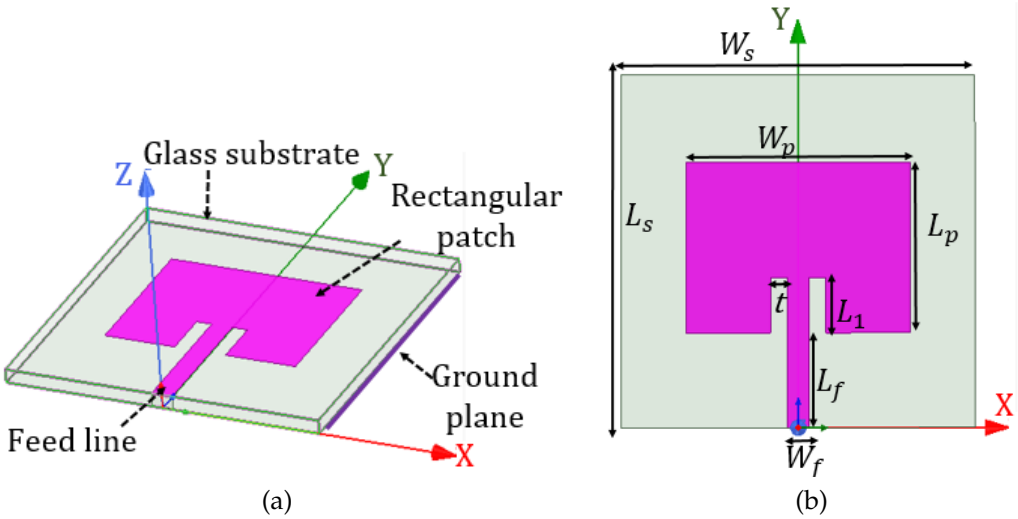

Figure 6. Rectangular patch antenna geometry (a) 3-D view, (b) top view. $W_s = 25mm$, $L_s = 25mm$, $L_p = 11.76mm$, $W_p = 15.8mm$, $t = 1mm$, $L_1 = 5.4mm$, $L_f = 5.8mm$, and $W_f = 1.77mm$.

3.2. Transparent antenna

The transparent antenna designed using the honeycomb-shaped mesh structure can be integrated into an OLED light source structure with minimal impact on the luminous efficiency. The proposed antenna was designed to cover the WLAN band but it can be operated on other bands by optimizing the mesh parameters. Fig. 7 shows the geometry of the mesh antenna with the honeycomb mesh dimensions. For easier comparison, the non-transparent and mesh antennas possess the same dimensions.

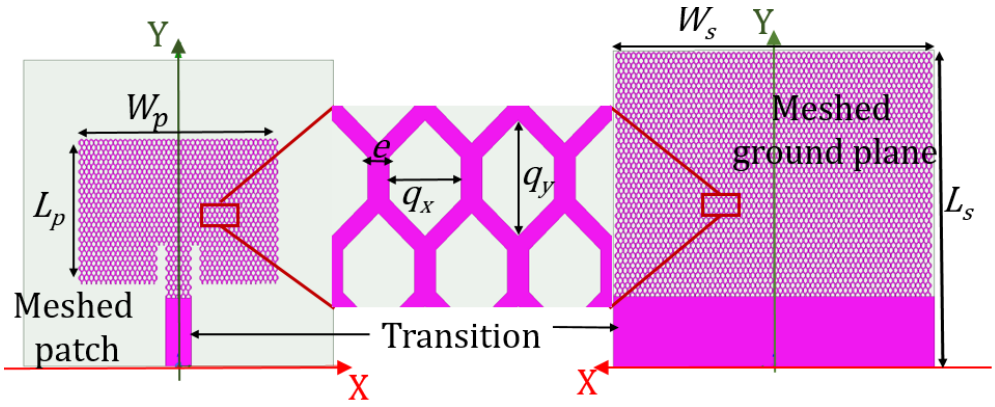

Figure 7. Transparent antenna geometry (a) meshed radiating patch, (b) mesh cells, and (c) meshed ground plane. $W_s = 25$ mm, $L_s = 25$ mm, $L_p = 11.76$ mm, $W_p = 15.8$ mm, $e = 50$ µm, $q_x = 320$ µm, and $q_x = 500$ µm

3.3. Comparison between the non-transparent and transparent antennas

Both design were simulated and analyzed using an electromagnetic solver, Ansys Electronics Desktop. The electrical and radiation parameters of the antennas are compared. Fig. 8 shows the comparison between the return losses for the compared antennas. For the two candidates, the antenna impedance's are well matched to 50Ω at the resonant frequency 5.15 GHz as the return losses are below 10 dB. The bandwidth defined by ($S_{11} \leq -10$ dB) are 130 MHz (5.19–5.32 GHz) for the non-transparent antenna and 110 MHz (5.09–5.2 GHz)

for the transparent antenna. It should be noted that the compared antennas have the same size; however, the disagreement noted between the resonance frequencies is justified by the resistance values for each structure (full *versus* mesh metallic layer).

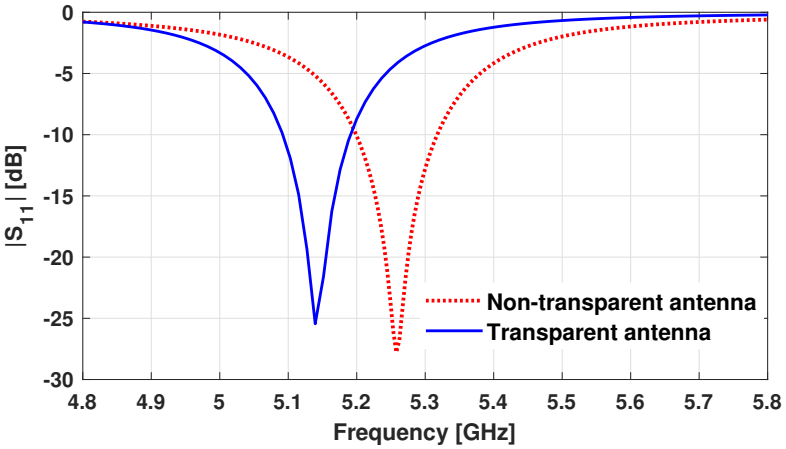

Figure 8. Comparison between the return losses of the compared antennas (non-transparent and transparent).

The radiation patterns for the two antennas are also compared in the Fig. 9. These diagrams are obtained for the resonant frequencies of each antenna and for the two planes; XZ-plane (Fig. 9 (a)) and YZ-plane (Fig. 9 (b)). These results are in acceptable agreement as the antennas size are equivalent. The peak gains are 6.23 dB and 5.5 dB for the non-transparent and transparent antennas, respectively. The two antennas achieved good gain in the operating band for WLAN applications. Therefore, increasing the sheet resistance value deteriorates the gain of the mesh antenna. This can be compensated by using meta-materials and applying array antenna techniques [37].

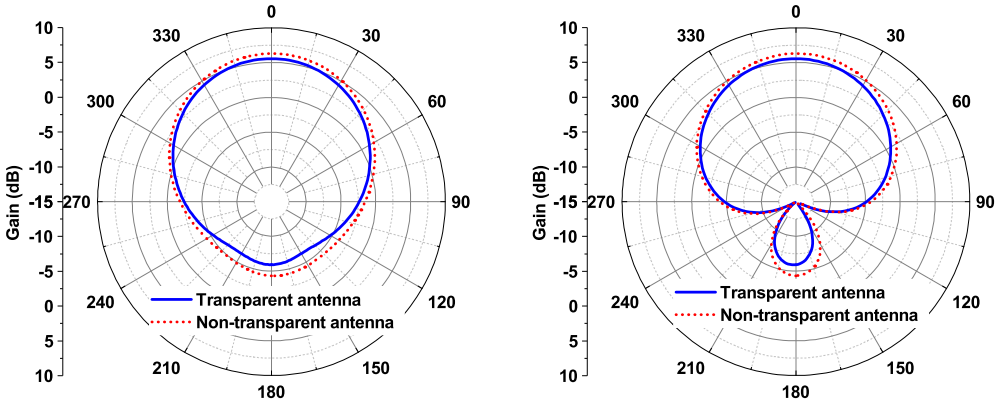

Figure 9. Comparison between the radiation patterns of the compared antennas; (a) XZ-plane and (b) YZ-plane.

4. Experimental results

The antennas are optimized using electromagnetic solver Ansys Electronics Desktop, and are manufactured by photolithography process to validate the results obtained in the simulation. Fig. 10 (a) illustrates photographs of the fabricated antennas. Their reflection coefficients and radiation patterns were measured. The former is evaluated using a Vector Network Analyzer. The latter is measured inside an anechoic chamber, as shown in Fig. 10(b).

(a) (b)

Figure 10. Manufactured antennas: (a) non-transparent and transparent antennas, (b) antenna measurement chamber setup.

4.1. Reflection coefficient comparison

The simulated and measured reflection coefficient of the non-transparent and transparent antennas are plotted in Fig. 11. The impedance matching of the manufactured transparent antenna is not well matched, this may be justified among other by inaccuracies of the mesh antenna fabrication process, electrical losses of the glass substrate and increased sheet resistance value due to the use of the mesh technique. In addition, the metal thickness $t = 370\,\text{nm}$ is as thin as to be comparable with the skin depth value 0.9 µm (calculated using the skin depth equation [21]), high loss is exhibited that reduces the antenna performances.

To minimise the losses due to skin depth, it is appropriated to use a metal thickness greater than $3 \times 0.9 = 2.7\,\mu\text{m}$. Nevertheless, the metal deposition technique used does not allow to obtain this thickness. However, the proposed antennas still exhibit acceptable impedance matching at the WLAN frequency band.

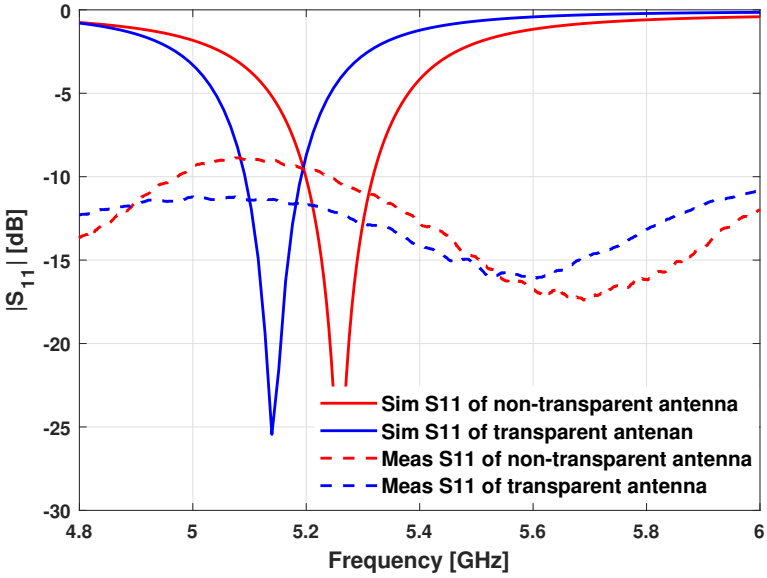

Figure 11. Measured and simulated return loss of the transparent and non-transparent antennas.

4.2. Radiation patterns comparison

The far-field radiation patterns of the non-transparent antenna at 5.27 GHz are shown in Fig. 12. Fig. 13 shows the far-field radiation patterns of the transparent antenna at 5.16 GHz. In general, the simulated results align with the measured results. The observed discrepancies are attributed to the fabrication issues and the electrical characteristics losses of the substrate. It is also observed that the antenna possess a mostly uni-directional radia-

tion pattern. The measured back radiation cannot be evaluated due to the measurement configuration of the anechoic chamber.

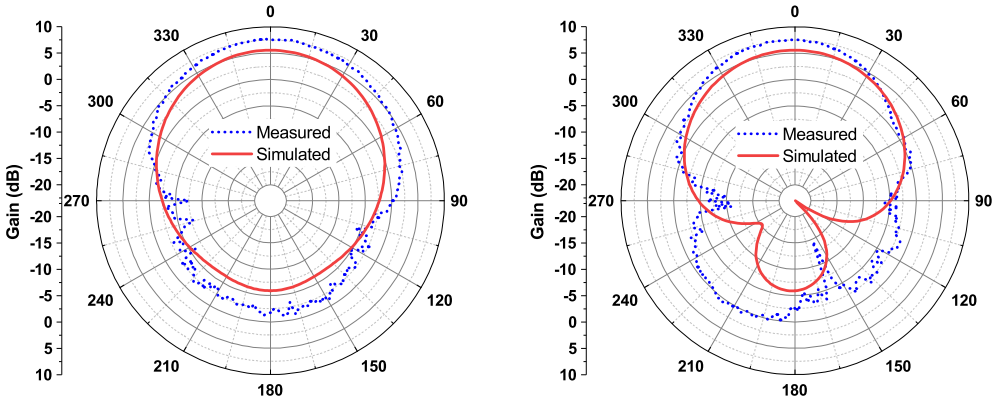

Figure 12. Measured and simulated radiation patterns of the non-transparent antenna, (a) in the XZ-plane and (b) in the YZ-plane.

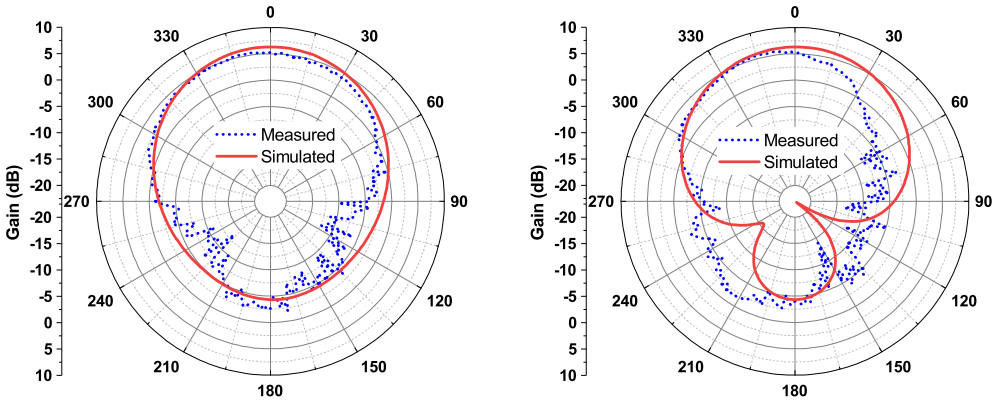

Figure 13. Measured and simulated radiation patterns of the transparent mesh antenna, (a) in the XZ-plane and (b) in the YZ-plane.

5. Antenna integration into OLEDs.

OLED becomes the most suitable technology in the future display and lighting systems, thanks to many benefits, such as high quality of light and image with excellent color rendering, low power consumption, controllability in terms of color temperature and the possibility to realize them on transparent or flexible substrate with lower manufacturing costs. The integration of antenna in this technology can provide a solution in terms of the implementation of future lighting systems and the coverage area in wireless communication. In [31], the authors discuss the use of transparent antennas for the future cities to improve network capacity, reduce visual pollution, and expand infrastructure in 5G wireless communication. These antennas will also be a good candidate for future 6G systems in which all possible communication scenarios will be found, such as terrestrial wireless communication networks, satellite communication, intelligent transport and massive Internet-of-Things (IoT) [38]. Therefore, this work aims to study the antennas integration in OLED technology to contribute to scientific research into the development of lighting systems.

The way of integrating transparent antenna into OLED technology will be discussed in this section. The OLED model parameters used in this study are the same ones in the

commercialized device [39]. In general, an OLED is made up of several organic layers located between two electrodes. Each layer has a specific role in the light emission process. Fig. 14 shows the OLED structure including the antenna placement. Fig. 14 (a) illustrates the various OLEDs components. Layer 1 is the 0.7 mm thick OLED glass substrate. Layer 2 is the ITO anode whose thickness is 150 nm. Layer 3 contains the Hole Transport Layer (HTL), Electron Transport Layer (ETL) and Emissive Layer (EML) with a thickness of 270 nm. Layer 4 is the metal cathode fabricated by aluminum and with a thickness of 120 nm. In order to protect the organic layers against oxidation, an encapsulation layer (layer 5) is implemented at the rear of the cathode. After encapsulation, the metal layer 6 is attached for heat dissipation. Fig. 14 (b) represents the overall size of the proposed OLED model. The antenna is replaced on the front of the OLED to minimize the effect of the metal layer on its radiation, as shown in the Fig. 14 (c). The yellowish aspect results from the camera settings as the white balance was not properly set.

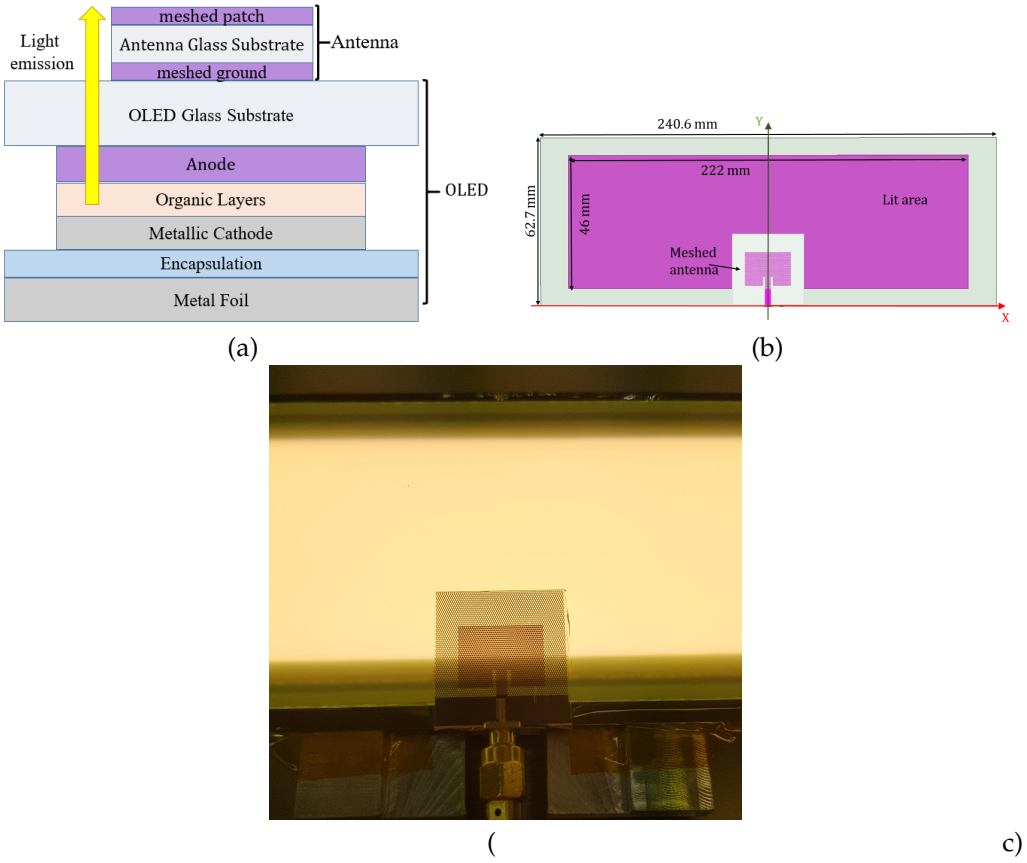

Figure 14. Antenna integration into OLED structure; (a) cross-sectional view, (b) top view and (c) in the measure step.

5.1. OLED effects on the antenna performances.

The comparison between the measured and simulated reflection coefficient of the antenna with and without OLED is shown in the Fig. 15. From this figure, it can be observed that an acceptable agreement between the results is obtained and the bandwidth can well cover the desired WLAN frequency band. The transparent antenna return loss is affected with OLED. The layers of the OLED also affect the antenna impedance and become less adapted in 50Ω. The resonant frequency of the proposed antenna shifts towards low frequencies with a narrow bandwidth.

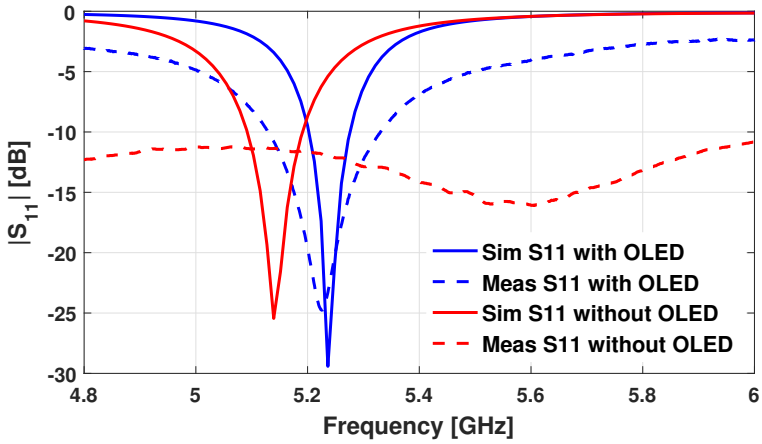

Figure 15. Comparison between measured and simulated return loss and with/without OLED.

Fig. 16 shows the comparison between the radiation patterns of the mesh antenna, with and without OLED: Fig. 16 (a) in the XZ-plane, Fig. 16 (b) in the YZ-plane and Fig. 16 (c) with OLED in 3D view. These diagrams are oriented along the direction of OLEDs light emission. The directivity and gain obtained of the antenna with OLEDs are 6.67 dBi and 4.86 dBi at 5.22 GHz, respectively. These values are improved after the integration of the OLED, this can be explained by the effect of the OLEDs layers, which are considered as a ground plane reflecting antenna radiation.

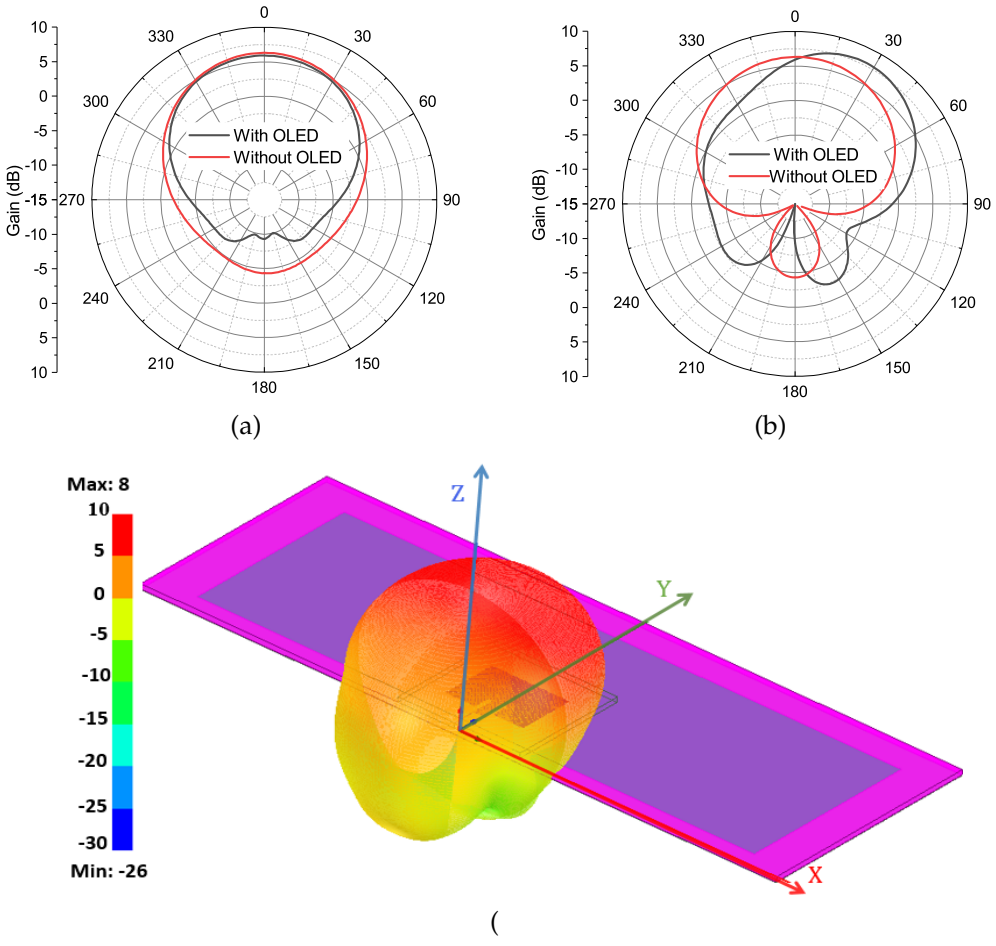

Figure 16. Radiation patterns of the transparent antenna with and without OLED; (a) in the XZ-plane, (b) in the YZ-plane and (c) with OLED in 3D view.

However, the materials used in the layers of the OLED light source are extremely critical for their efficiency and lifetime. The OLED panels contain ITO and aluminum electrodes and metal foil layer that acts as a reference ground for the antenna. The slight differences between the two results with and without OLED can be interpreted by the effect of these layers on the antenna radiation. Since, the size of the layers is much greater than the integrated antenna size, these layers act as a large ground plane. This ground plane allows electromagnetic waves from the surface to be confined within the OLED panel rather than radiating outwards. Therefore, these fields affect the electrical and radiation performance of the antenna.

5.2. Antenna effects on the OLED colorimetric parameters.

After the study of the effects of the OLED on the radio-electrical parameters of the antenna, it is very important to investigate the influence of this integration on the color appearance of OLED. Therefore, optical and photometric characterizations for the OLED were performed before and after the antenna integration. Fig. 17 shows photograph of the optical and photonic measurements of OLED. These measurements were performed on an optical bench at ambient temperature with the spectroradiometer MINOLTA CS-1000. This measuring device is placed at 1 m from the OLED allowing the measurement of optical and colorimetric parameters in the visible field $[380 - 780\,\text{nm}]$ with a 1 nm step. The measurements were made for both cases with and without antenna and were repeated 21 times in order to ensure the accuracy of the measured values.

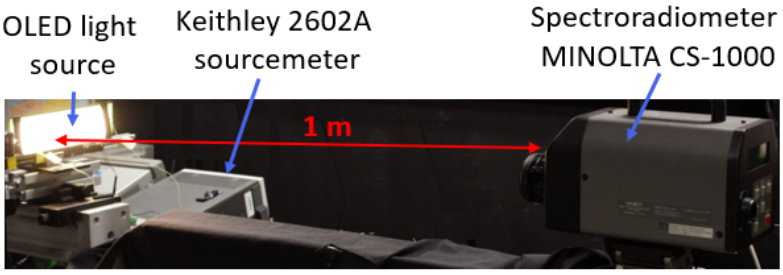

Figure 17. Measuring bench for the optical characterizations.

Then, the colorimetric parameters were calculated using IES TM-30-18 color rendering method [40]. The use of this method is more appropriate for LED and OLED light sources, because it generates more colorimetric analysis than the CIE fidelity index method. It is consists of calculating the mean fidelity index (Rf) by the light source rendering test using 99 Color Evaluation Samples (CES) compared with the CIE (Commission Internationale de l'Éclairage) [41], Which considers only 8 Test Color Samples (TCS) to calculate Ra (Ra: Color rendering index calculated based on CIE 1995 CRI method). The colorimetric parameters such as Spectral Power distribution (SPD), Correlated Color Temperature (CCT), (x,y) coordinates, (u',v') coordinates, Duv value (the distance between the (u',v') chromaticity coordinate of OLED and the planckian locus on the CIE 1976 color space), Rf (fidelity index) and Rg (Gamut Index) were calculated to understand the color appearance shifting of OLED after antenna integration.

Fig. 18 illustrates a comparison between the SPD of a Warm White OLED (CCT = 3000 K), and the SPD of the OLED measured with the integrated antenna. It is noticed that the SPD changes after the antenna integration. A variation in the SPD generally leads to changes in colorimetric parameters.

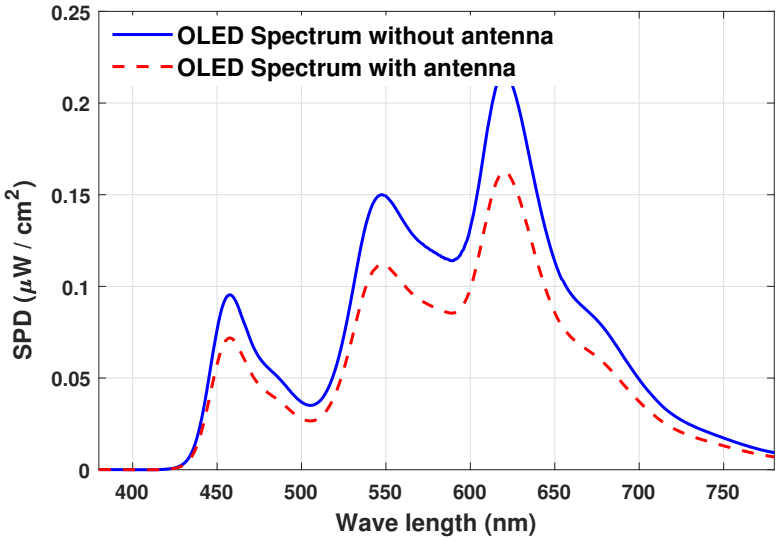

Figure 18. The SPD of the OLED with and without mesh transparent antenna.

Average of the CCT, (x,y) coordinates, (u',v') coordinates, Duv value, Rf and Rg are presented in Table. 2 for both cases with and without antenna. According to the MacAdam ellipse, slight differences observed in these parameters are not detectable by users. Hence, the measures show no significant difference between the these parameters with and without antenna. However, the luminance value decreased by 25 % after antenna integration, therefore this alteration will lead to a non-uniformity at the lamp luminosity.

Table 2. Measured colorimetric parameters of the OLED before and after antenna integration.

Colorimetric parameters	Without antenna	With antenna
Luminance [cd m^{-2}]	8654 $\pm$ 12.3	6481 $\pm$ 8.3
CCT [K]	3037 $\pm$ 3.6	3033 $\pm$ 0.3
(x , y)	(0.4331 , 0.4006)	(0.4330 , 0.3998)
(u' , v')	(0.2496 , 0.5194)	(0.2498 , 0.5191)
Duv	-0.0009	-0.0011
(Rf, Rg)	(86 , 99)	(86 , 99)

6. Conclusions and perspectives

To the author's knowledge, this paper has proposed for the first time an original contribution with the experiment tests to integrate a transparent antenna into an OLED light source. The discussed method first involves designing a honeycomb mesh which achieves optical transparency. With the chosen mesh parameters, this transparency is about 75.4 % while the antenna is not visible to the bare eye. This antenna is fabricated using a photolithography process and compared with its non-transparent counterpart in terms of the S-parameters and radiation patterns measured inside an anechoic chamber.

Furthermore, the optical and photometric characterizations were performed with and without antenna. The luminance, spectral power distributions, correlated color temperature, CIE 1931 (x,y), CIE1976 (u',v'), Duv value, fidelity and gamut indexes have been calculated using the IES TM-30-18 color rendering method. It has been evaluated that the integration of the three-layers antenna degrades the luminance of OLED by 25 % due to the chosen substrate and mesh dimensions.

Optically transparent antennas enable replacement of conventional antennas in future devices. With the development of connected and intelligent objects, presented in all sectors such as smart city, smart lighting, transport, wearables, industry, smart hospitals, etc., these antennas will be crucial in future 6G applications. Therefore, future work will aim at improving the co-integration mechanism using some OLED layers as support and radiating elements for the antenna. On the one hand, this will optimize the fabrication cost by

reducing the number of supplemental added layers. On the other hand, by minimizing the number of interfaces, this will reduce transmission losses due to refraction index mismatches, maximizing luminous efficiency.

Funding: This work is supported by PHC Maghreb (Hubert Curien Program, Grant number: 43981ZG) "MELINA" (Mastering Efficient Lighting in North Africa) supported by the French Ministry of Europe and Foreign Affairs and Campus France and, in Morocco, by the Ministry of Higher Education, Scientific Research and Innovation, in partnership with the National Center for Scientific and Technical Research (CNRST).

Data Availability Statement: Data will be provided upon request from the corresponding author.

Acknowledgments: The authors would like to express their sincere gratitude to Benoit Schlegel and Pierre Hernandez of the LAPLACE lab for their support in the antenna manufacturing. .

Conflicts of Interest: The authors declare no conflict of interest.

References

1. Zissis, G.; Bertoldi, P.; Serrenho, T. Update on the Status of LED-Lighting world market since 2018. In Publications Office of the European Union:, Luxembourg, 2021.
2. Zissis, G.; Dupuis, P.; Canale, L.; Pigenet, N. Smart lighting systems for smart cities. *Holistic Approach for Decision Making Towards Designing Smart Cities*, Springer. **2021**, 75–92.
3. Green, R. B.; Guzman, M.; Izyumskaya, N.; Ullah, B.; Hia, S.; Pitchford, J.; Timsina, R.; Avrutin, V.; Ozgur, U.; Morkoc, H. et al . Optically transparent antennas and filters: A smart city concept to alleviate infrastructure and network capacity challenges. *IEEE Antennas and propagation magazine* **2019**, 37–47.
4. EL Halaoui, M.; Canale, L.; Asselman, A.; Zissis, G. An optically transparent antenna integrated in OLED light source for 5G applications. In 2020 IEEE International Conference on Environment and Electrical Engineering and 2020 IEEE Industrial and Commercial Power Systems Europe (EEEIC/ICPS Europe) (June 2020).
5. Park, J.; Park, D.; Kim, M.; Jung, D.; You, C.; Choi, D.; Lee, J.; Hong, W. Circuit-on-Display: A Flexible, Invisible Hybrid Electromagnetic Sensor Concept. *IEEE Journal of Microwaves* **2021**, vol. 1, no. 2, 550–559.
6. Silva, Z. J.; Valenta, C. R.; Durgin, G. Optically transparent antennas: A survey of transparent microwave conductor performance and applications. *IEEE Antennas and Propagation Magazine* **2020**, vol. 63, no. 1, 27–39.
7. Lee, S. Y.; Choo, M.; Jung, S.; Hong, W. Optically transparent nanopatterned antennas: A review and future directions. *Applied Sciences* **2018**, vol. 8, no. 6, 901.
8. Sayem, A. S. M.; Lalbakhsh, A.; Esselle, K. P.; Esselle, J. L.; Buckley, B.; O'Flynn, B.; Simorangkir, R. B. Flexible transparent antennas: Advancements, challenges, and prospects. *IEEE Open Journal of Antennas and Propagation* **2022**, vol. 3, 1109–1133.
9. Ali, N.M.; Misran, N.; Mansor, M.; Jamlos, M. Transparent solar antenna of 28 GHz using transparent conductive oxides (TCO) thin film. *Journal of Physics: Conference Series* **2017**, vol. 852, no. 1, 012036.
10. Cai, L. An on-glass optically transparent monopole antenna with ultrawide bandwidth for solar energy harvesting. *electronics* **2019**, vol. 8, no. 9, 916.
11. Potti, D.; Tusharika, Y.; Alsath, M. G. N.; Kirubaveni, S.; Kanagasabai, M.; Sankararajan, R.; Narendhiran, S.; Bhargav, P. B. A novel optically transparent UWB antenna for automotive MIMO communications. *IEEE Transactions on Antennas and Propagation* **2021**, vol. 69, no. 7, 3821–3828.
12. Lai, S.; Wu, Y.; Zhu, X.; Gu, W.; Wu, W. An optically transparent ultrabroadband microwave absorber. *IEEE photonics journal* **2017**, vol. 9, no. 6, 1–10.
13. Thampy, A. S.; Dhamodharan, S. K. Performance analysis and comparison of ITO-and FTO-based optically transparent terahertz U-shaped patch antennas. *Physica E: Low-dimensional Systems and Nanostructures* **2015**, vol. 66, 52–58.
14. Wu, C. T.; Ho, Y. R.; Huang, D. Z.; Huang, J. J. AZO/silver nanowire stacked films deposited by RF magnetron sputtering for transparent antenna. *Surface and Coatings Technology* **2020**, vol. 360, 95–102.
15. Song, H. J.; Hsu, T. Y.; Sievenpiper, D. F.; Hsu, H. P.; Schaffner, J.; Yasan, E. A method for improving the efficiency of transparent film antennas. *IEEE Antennas and Wireless Propagation Letters* **2020**, vol. 7, 753–756.
16. Azini, A. S.; Kamarudin, M. R.; Rahman, T. B. A.; Iddi, H. U.; Abdulrahman, A. Y.; Jamlos, M. F. Transparent antenna design for WiMAX application. *Progress In Electromagnetics Research* **2013**, vol. 138, 133–141.
17. Desai, A.; Upadhyaya, T.; Palandoken, M.; Gocen, C. Dual band transparent antenna for wireless MIMO system applications. *Microwave and Optical Technology Letters* **2019**, vol. 61, no. 7, 1845–1856.
18. Desai, A.; Upadhyaya, T.; Patel, R. Compact wideband transparent antenna for 5G communication systems. *Microwave and Optical Technology Letters* **2019**, vol. 61, no. 3, 781–786.
19. Desai, A.; Palandoken, M.; Elfergani, I.; Akdag, I.; Zebiri, C.; Bastos, J.; Rodriguez, J.; Abd-Alhameed, R. A. Transparent 2-element 5G MIMO antenna for sub-6 GHz applications. *Electronics* **2022**, vol. 11, no. 2, 251.

20. Yasin, T.; Baktur, R.; Furse, C. A comparative study on two types of transparent patch antennas. 2011 XXXth URSI General Assembly and Scientific Symposium, Istanbul, Turkey, 13-20 August 2011, 1–4.
21. Martin, A.; Gautier, C.; Castel, X.; Himdi, M. Transparent and miniature FM antenna in printed technology. *International Journal of Microwave and Wireless Technologies* **2018**, vol. 10, no. 1, 19–24.
22. Hautcoeur, J.; Castel, X.; Colombel, F.;Benzerga, R.; Himdi, M.; Legeay, G.; Motta-Cruz, E. Transparency and electrical properties of meshed metal films. *Thin Solid Films* **2011**, vol. 519, no. 11, 3851–3858.
23. Dao, Q. H.; Grundmann, L.; Geck, B. Optically Transparent 24 GHz Analog Front-End Based on Meshed Microstrip Lines for the Integration in a Self-Sufficient RFID Sensor Tag. *IEEE Journal of Radio Frequency Identification* **2019**, vol. 4, no. 2, 83–92.
24. Yu, P. C.; Hong, C. C.; Liou, T. M. Bendable transparent conductive meshes based on multi-layer inkjet-printed silver patterns. *Journal of Micromechanics and Microengineering* **2016**, vol. 26, no. 3, 035012.
25. Kang, S. H.; Jung, C. W. Transparent patch antenna using metal mesh. *IEEE Transactions on Antennas and Propagation* **2018**, vol. 66, no. 4, 2095–2100.
26. Martin, A.; Castel, X.; Himdi, M.; Lafond, O. Mesh parameters influence on transparent and active antennas performance at microwaves. *AIP Advances* **2011**, vol. 7, no. 8, 085120.
27. Zhang, Y.; Shen, S.; Chiu, C. Y.; Murch, R. Hybrid RF-solar energy harvesting systems utilizing transparent multiport micromeshed antennas. *IEEE Transactions on Microwave Theory and Techniques* **2019**, vol. 67, no. 11, 4534–4546.
28. Hautcoeur, J.; Colombel, F.; Castel, X.; Himdi, M.; Cruz, E. M. Radiofrequency performances of transparent ultra-wideband antennas. *Progress In Electromagnetics Research C* **2011**, vol. 22, 259–271.
29. Hong, W.; Lim, S.; Ko, S.; Kim, Y. G. Optically invisible antenna integrated within an OLED touch display panel for IoT applications. *IEEE Transactions on Antennas and Propagation* **2017**, vol. 65, no. 7, 3750–3755.
30. Hong, W.; Ko, S.; Kim, Y. G.; Lim, S. Invisible antennas using mesoscale conductive polymer wires embedded within OLED displays. In 2017 11th European Conference on Antennas and Propagation (EUCAP), Paris, France, 19-24 March 2017.
31. Park, J.; Lee, S. Y.; Kim, J.; Park, D.; Choi, W.; Hong, W. An optically invisible antenna-on-display concept for millimeter-wave 5G cellular devices. *IEEE Transactions on Antennas and Propagation* **2019**, vol. 67, no. 5, 2942–2952.
32. Kim, M.; Lee, D.; Oh, Y.; Lee, J. Y.; Kim, B.; Park, J.; Park, D.; Hong, W. Antenna-on-display concept on an extremely thin substrate for sub-6 GHz wireless applications. *IEEE Transactions on Antennas and Propagation* **2022**, vol. 70, no. 7, 5929–5934.
33. El Halaoui, M.; Canale, L.; Asselman, A.; Zissis, G. Design and Analysis of Transparent and Non-Transparent Antennas Integrated in OLEDs at 3.5 GHz Band for 5G Applications. In 2021 IEEE International Conference on Environment and Electrical Engineering and 2021 IEEE Industrial and Commercial Power Systems Europe (EEEIC/ICPS Europe), Bari, Italy, 07-10 September 2021.
34. El Halaoui, M.; Canale, L.; Dupuis, P.; Asselman, A.; Zissis, G. An Optically Transparent Mesh-Antenna Integrated in OLEDs for WLAN Applications. In 2021 IEEE Industry Applications Society Annual Meeting (IAS), Vancouver, BC, Canada, 10-14 October 2021.
35. Charman, W. N. Static accommodation and the minimum angle of resolution. *American journal of optometry and physiological optics* **1986**, vol. 63, no. 11, 915–921.
36. Balanis, C. A. *Antenna theory: analysis and design*, 4th ed.; John wiley sons, 2016.
37. Kaabal, A.; El Halaoui, M.; Amhaimar, L.; Azizi, S.; Dellaoui, S.; Ahyoud, S.; Asselman, A. Array antenna design with dual resonators 1D-EBG for enhancement of directivity and radiation bandwidth. *International Journal of Microwave and Optical Technology* **2019**, vol. 14, no. 4, 231–239.
38. Ikram, M.; Sultan, K.; Lateef, M. F.; Alqadami, A. S. A road towards 6G communication—A review of 5G antennas, arrays, and wearable devices. *Electronics* **2022**, vol. 11, no. 1, 169.
39. Lumiblade OLED Panel Brite FL300, . Available online: https://www.oledworks.com/wpcontent/uploads/2016/03/Data-sheet-Lumiblade-OLED-Panel-BriteFL300L-ww-wm-1.pdf.
40. Abdellah, O. B.; Al Haddad, A.; El Halaoui, M.; Dupuis, P.; Canale, L.; Asselman, A.; Zissis, G. Colorimetric Characterizations of Large Area White OLEDs Under Thermal And Electrical Stress Using TM-30-18 Method. In 2020 Fifth Junior Conference on Lighting (Lighting), Ruse, Bulgaria, 24-26 September 2020.
41. Commission Internationale de l'Eclairage: Method of measuring and specifying colour rendering properties of light sources: Technical report: CIE 013.3-1995. Available online: https://cie.co.at/publications/method-measuring-and-specifying-colour-rendering-properties-light-sources.